Progress In Electromagnetics Research B, Vol. 34, 15–30, 2011

THEORY OF GAIN ENHANCEMENT OF UC-PBG ANTENNA STRUCTURES WITHOUT INVOKING MAXWELL'S EQUATIONS: AN ARRAY SIGNAL PROCESSING APPROACH

T. A. Elwi [1, *], H. M. Al-Rizzo [1], N. Bouaynaya [1], M. M. Hammood [2], and Y. Al-Naiemy [2]

[1]Department of Systems Engineering, George W. Donaghey College of Engineering and Information Technology, University of Arkansas at Little Rock, Little Rock, AR 72204, USA

[2]Department of Applied Science, University of Arkansas at Little Rock, Little Rock, AR 72204, USA

Abstract—In this paper, a novel and computationally efficient algorithm which combines Array Signal Processing (ASP) approach with Fourier Optics (FO) is developed in the realm of gain enhancement achieved by placing Uniplanar Compact-Photonic Band Gap (UC-PBG) structures on top of microstrip antennas. The proposed scheme applies FO to the well-known sampling theorem borrowed from Digital Signal Processing (DSP) analysis in the framework of ASP approach which we refer to as the FDA algorithm. The FDA algorithm is suitable for lossless UC-PBG structures with 1-D, 2-D and 3-D lattice of canonical geometrical apertures, such as circular, octagonal, hexagonal, and square. In order to validate the proposed approach, two different UC-PBG structures of octagonal and circular apertures are considered at 2.6 GHz. The UC-PBG structures under consideration consist of two layers positioned above a microstrip antenna; each layer is an array of 9×9 apertures separated by half of the focal length distance of the lens in the near-field of the microstrip antenna. The performance of the microstrip antenna with and without the UC-PBG is reported using numerical simulations performed using CST Microwave Studio (CST MWS) based on the Finite Integration Technique (FIT). The radiation patterns and directivity of the microstrip antenna based on UC-PBG structures are evaluated using the proposed FDA algorithm and

Received 27 June 2011, Accepted 17 August 2011, Scheduled 20 August 2011

* Corresponding author: Taha A. Elwi (taelwi@ualr.edu).

validated against numerical results obtained from CST MWS where an excellent agreement is found between the FDA algorithm and the 3-D full wave simulations. The UC-PBG structure of octagonal apertures provides a remarkable enhancement in the bore-sight gain of about 7.8 dBi at 2.6 GHz with respect to that obtained from the conventional microstrip antenna, while the circular apertures provide gain enhancement in excess of 10 dBi above the gain of the same microstrip antenna.

1. INTRODUCTION

Photonic Band-Gap (PBG) or Electromagnetic Band-Gap (EBG) structures arose from classical concepts of optics [1]. The applications of these structures have been extended to antennas and passive components operating in the microwave frequency regime [2]. Analysis of PBG/EBG structures used to enhance the gain of antennas has been reported using a variety of numerical formulations based on the direct solution of Maxwell's equations [2–9]. Recently, we proposed an algorithm to optimize the position of the UC-PBG structure by applying ray tracing and refraction concepts in order to achieve maximum bore-sight gain and front-to-back (F/B) ratio [9]. It should be noted that in most of the previously reported studies [3–8], the PBG design was achieved by iteratively solving Maxwell's equations to optimize the interaction between the antenna and the UC-PBG structure. However, parametric and/or optimization studies conducted using rigorous numerical simulations based on solving Maxwell's equations in the time and/or frequency domain are costly in terms of simulation times and CPU requirements. This is in contrast to the proposed approach, which is simpler, faster, and more physically appealing.

Most of the directive photonic-based antennas are constructed from a number of layers of different dielectric permittivity as in Bragg mirrors or from alumina rods or thin cylindrical metal wires [6]. Increasing the number of periodicity of these layers leads to a pencil-like beam from a patch antenna [7]. In [7], a Fabry Perot cavity was used to reflect radiation in order to realize Gaussian-beamlike directive antennas. A planar microstrip array with two substrate layers of a common ground plane has been used to focus the electromagnetic beam toward a small spot with a predetermined distance in the near-field zone of the array [6] and [7].

In this paper, we present a novel algorithm based on FO and ASP in order to analyze a UC-PBG structure based on a periodical uniform repetition of arbitrarily-shaped apertures on a planar conducting plane.

The two well-known UC-PBG structures reported in [8] and [9] are used to validate the proposed algorithm. The first example, reported in [8], is a UC-PBG structure based on array of circular apertures, whereas the UC-PBG structure in [9] is based on octagonal apertures. The UC-PBG structure of circular apertures is applied to a microstrip antenna resonating at 2.6 GHz. The same microstrip antenna is considered using a UC-PBG structure consisting of octagonal apertures. The rest of the paper is organized as follows. Section 2 presents the mathematical formulation of the proposed FDA algorithm. The design methodology is discussed in Section 3. Section 4 validates results obtained from the FDA algorithm against numerical simulations using CST MWS. Finally, the conclusions are summarized in Section 5.

2. MATHEMATICAL FORMULATION

Common UC-PBG structures consist of a number of UC-PBG layers separated by a certain distance [4]. An individual UC-PBG layer is designed using a specific number of unit cells. Each individual cell is an aperture which we will consider as a *spatial filter* of a certain Impulse Response (IR). Mathematically, the periodicity of these apertures can be represented by an impulse train function. The UC-PBG layer is modeled by the convolution of the periodic function with the IR of individual apertures.

2.1. DSP Approach to Solve the Periodicity Function of the UC-PBG Structure

We assume a 2-D UC-PBG structure, which consists of any number of periodical, arbitrarily-shaped apertures of constant separation, as shown in Figure 1.

The UC-PBG structure is assumed to be cascaded with an arbitrary number of layers S_o. The individual aperture has unit cell function (F_{uc}) with 2-D periodicity (N, M). The summation of these apertures can be represented in the time domain as

$$f_{SL}[x,y] = \sum_{n=-N/2}^{N/2} \sum_{m=-M/2}^{M/2} f_{uc}(x-nX,\, y-mY) \tag{1}$$

Next, the frequency response of the UC-PBG layer, defined as the Fourier transform of the IR response, is given by

$$F_{SL}(v_x,v_y) = \underbrace{F_{uc}(v_x,v_y)}_{IR} \underbrace{\left[\frac{\sin(\pi v_x(N+1)X)}{\sin(\pi v_x X)}\right]\left[\frac{\sin(\pi v_y(M+1)Y)}{\sin(\pi v_y Y)}\right]}_{\text{Layer Envelop Function}} \tag{2}$$

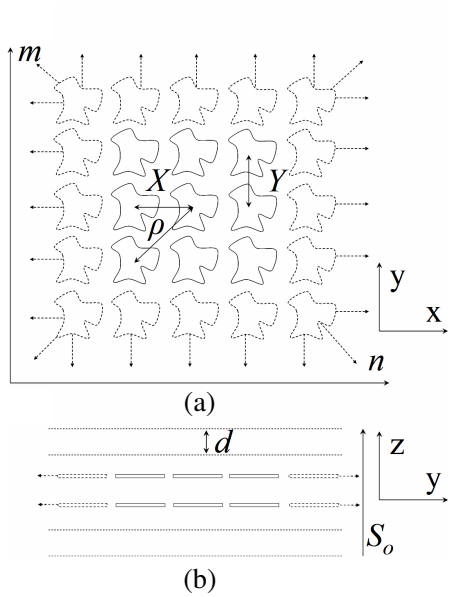

Figure 1. Conceptual UC-PBG structure. (a) Top view and (b) side view.

where, v_x and v_y are the spatial frequencies along the x- and y-directions, respectively. X and Y are the interval displacements along the x- and y-directions, respectively. The proof of Equation (2) is provided in the Appendix A. The Layer Envelop Function (LEF), as marked in Equation (2), is called for a single UC-PBG layer. Equation (2) can be expressed as

$$F_{SL}\left(v_x, v_y\right) = F_{uc}\left(v_x, v_y\right) K(N, M) \tag{3}$$

where $K(N,M) = [\frac{\sin(\pi v_x(N+1)X)}{\sin(\pi v_x X)}][\frac{\sin(\pi v_y(M+1)Y)}{\sin(\pi v_y Y)}]$ is the Brillouin zone vector position.

The normalized F_{SL} in Equation (2) is

$$F_{SL}(v_x, v_y)_n = \frac{F_{uc}(v_x, v_y)}{NM}\left[\frac{\sin(\pi v_x(N+1)X)}{\sin(\pi v_x X)}\right]\left[\frac{\sin(\pi v_y(M+1)Y)}{\sin(\pi v_y Y)}\right] \tag{4}$$

Since the UC-PBG is a memory less system; the center can be located at any position (n_0, m_0). Hence, Equation (4) can be generalized as

$$F_{SL}(v_x, v_y) = \frac{F_{uc}(v_x, v_y)}{NM}\left[\frac{\sin(\pi v_x(N-n_o+1)X)}{\sin(\pi v_x X)}\right] \left[\frac{\sin(\pi v_y(M-m_o+1)Y)}{\sin(\pi v_y Y)}\right] \tag{5}$$

Substituting for $v_x = v_y = x/\lambda d$, where λ is the wave length and d is the distance between the aperture and the observation point, and $N = M$, Equation (3) becomes

$$F_{SL}(v_x, v_y) = F_{uc}(v_x, v_y) \left[\frac{\sin\left(\frac{\pi x X}{\lambda d}(N+1)\right)}{\sin\left(\frac{\pi x X}{\lambda d}\right)} \right]^2 \tag{6}$$

In Equation (4), if the argument $(\pi x X/\lambda d) \ll 1$ in the far field region, therefore, for good approximation

$$F_{SL}(v_x, v_y) \approx F_{uc}(v_x, v_y) \left[\frac{\sin\left(\frac{\pi x X}{\lambda d}(N+1)\right)}{\left(\frac{\pi x X}{\lambda d}\right)} \right]^2 \tag{7}$$

For a single UC-PBG layer, the far-field diffraction pattern is

$$g_S(x, y) = h_S F_{SL}[v_x, v_y] \tag{8}$$

where h_s is the transfer function of free space given by [10]

$$h_S = (j/\lambda d_S) \exp(-jkd_S) \tag{9}$$

By cascading an arbitrary number S_o of UC-PBG layers, where S_o is along the z-direction, the overall effective far-field diffraction pattern is the envelope multiplication of the far field diffractions functions of the UC-PBG layers. According to the ray tracing matrix for the optical path theorem in [12], the final far-field diffraction pattern from the 3-D Fourier transformation $g_{total}(x, y, z)$ is

$$g_{total}(x, y, z) = g_1(x, y) \cdot g_2(x, y) \ldots g_{S_o}(x, y) \tag{10}$$

Since the UC-PBG layer is a LTI system, cascading an arbitrary number S_o of UC-PBG layers can be accounted by the multiplication of the functions of the UC-PBG layers as shown below

$$g_{total}(x, y, z) = \prod_{S=1}^{S_o} h_S F_{SL}(v_x, v_y) \tag{11}$$

2.2. Fourier Optics to Find the Function of Individual Unit Cell

Two different unit cell geometries with octagonal and circular-shaped apertures are analyzed. We define the aperture function (F_{uc}) using FO. The full derivations for each geometry are presented in the following.

The geometry of the octagonal aperture is shown in Figure 2(a). The octagon is decomposed into four rectangular slits rotated by 45° as seen in Figure 2. The formulation starts by applying the FO

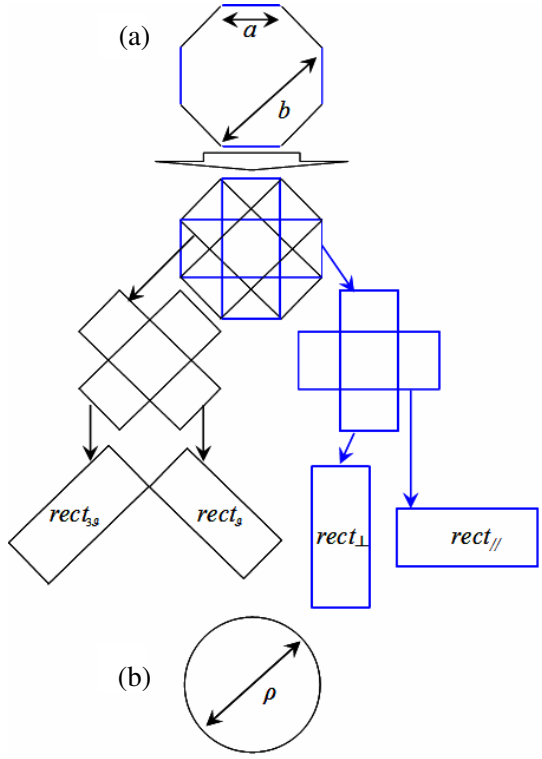

Figure 2. The proposed aperture. (a) Decomposition strategy of the unit cell of the octagonal aperture and (b) the circular aperture.

transformation to a single rectangular slit. The diffraction pattern of a single rectangular slit with width (a) and length (b) as follows

$$\begin{aligned} rect_{//} &= a\,\mathrm{sin}\,c\,(av_x)b\,\mathrm{sin}\,c\,(bv_y) \\ rect_{\perp} &= b\,\mathrm{sin}\,c\,(bv_x)a\,\mathrm{sin}\,c\,(av_y) \end{aligned} \tag{12}$$

Equation (2) can be re-written for the diagonal slits that are oblique with angle $\vartheta = 45^\circ$ and $3\vartheta = 135^\circ$ using Johnson transformation [10] which leads to

$$\begin{aligned} rect_{\vartheta} =& a\,\mathrm{sin}\,c(av_x)b\,\mathrm{sin}\,c(bv_y)\,\mathrm{cos}(\vartheta) \\ &+ b\,\mathrm{sin}\,c(bv_x)a\,\mathrm{sin}\,c(av_y)\,\mathrm{sin}(\vartheta) \\ rect_{3\vartheta} =& -a\,\mathrm{sin}\,c(av_x)b\,\mathrm{sin}\,c(bv_y)\,\mathrm{sin}(3\vartheta) \\ &+ b\,\mathrm{sin}\,c(bv_x)a\,\mathrm{sin}\,c(av_y)\,\mathrm{cos}(3\vartheta) \end{aligned} \tag{13}$$

Next, we generalize the analysis to cases involving an arbitrary number of slits and angles as a Fourier summation of a specific number

of slits as shown below

$$F_{uc}(v_x, v_y) = rect_{\perp} rect_{//} rect_{\vartheta} rect_{3\vartheta} \tag{14}$$

and for any geometry as

$$F_{uc}(v_x, v_y) = \prod_{p=1}^{p_o} \begin{bmatrix} \cos(p\vartheta) & \sin(p\vartheta) \\ -\sin(p\vartheta) & \cos(p\vartheta) \end{bmatrix} \begin{bmatrix} a\sin c(\pi a v_x) & b\sin c(\pi b v_y) \\ b\sin c(\pi b v_x) & a\sin c(\pi a v_y) \end{bmatrix} \tag{15}$$

where, $\vartheta = 180^{\circ}/p_o$ and p_o is the half number of the aperture sides. For cross geometry, $p_o = 2$, for hexagon, $p_o = 3$, and for octagon, $p_o = 4$.

For the circular aperture shown in Figure 2(b), Equation (15) can be reduced by applying Bessel Fourier Transformation [12] when $p_o \to \infty$ into

$$\begin{aligned} F_{uc}(v_x, v_y) &= \frac{2J_1(\pi D v_\rho)}{\pi D v_\rho} \\ v_\rho &= \frac{\rho}{\lambda d}, \quad \rho = (x^2 + y^2)^{1/2} \end{aligned} \tag{16}$$

where, D is displacement interval in the x- and y-directions and ρ is the diameter of the circular aperture.

The directivity is evaluated from the UC-PBG IR functions using the familiar definition of radiation intensity which is given as [9]

$$U(x, y, z) = U_o \left| g_{total}(x, y, z) \right|^2 \tag{17}$$

where, U_o is the electromagnetic intensity $(W/4\pi)$ of an isotropic radiator. To convert from Cartesian to spherical coordinate system, the following relations can be used

$$\begin{aligned} \theta &= \sin^{-1}(x/d) \\ \phi &= \sin^{-1}(y/d) \end{aligned} \tag{18}$$

The directivity derived from the total intensity in spherical coordinate system is given by

$$D = \frac{U(\theta, \phi)}{U_0} = \frac{4\pi U(\theta, \phi)}{P_{rad}} \tag{19}$$

where, U_o is the electromagnetic intensity of an isotropic radiator.

3. UC-PBG DESIGN METHODOLOGY

In this section; firstly, the principle of operation of the UC-PBG structures is explained based on optical concepts using ray tracing and Snell's law [10]. Next, the design parameters of both UC-PBG designs that were suggested in [10] and [11] are provided.

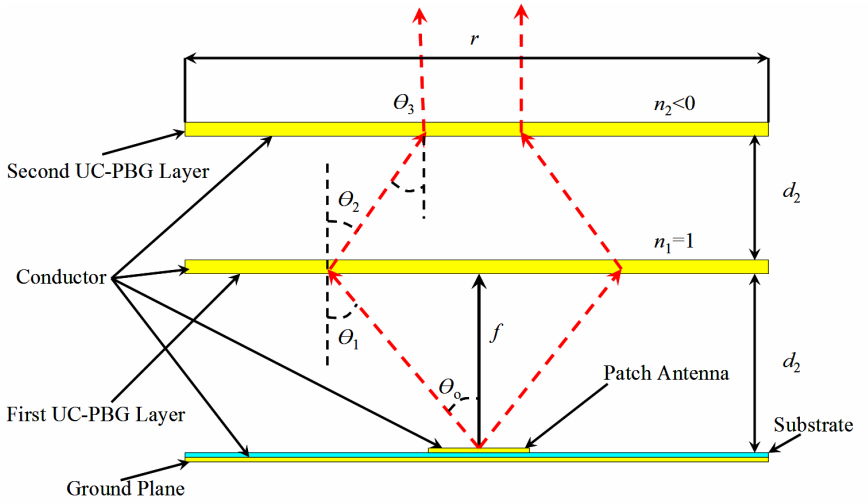

Figure 3. Ray tracing model of a UC-PBG antenna structure based on Snell's law.

3.1. Ray Tracing and Classical Optics Analysis

Starting from classical optics, the refractive index, angle of the incident radiation, position of the source with respect to the UC-PBG layers and focal length of the UC-PBG lens, the Half Power Beam-Widths (HPBWs) can be determined using ray tracing analysis and Snell's law [9]. The bore-sight gain can be evaluated using the HPBWs empirical relation reported in [9]. Based on this relationship, it is found that the antenna gain is inversely proportional to the refraction angles with respect to each layer as conceptualized in Figure 3. Applying ray tracing analysis to the UC-PBG lenses, it is found that the lens has to be placed at a distance equal to the focal length to generate paraxial beam rays with respect to the lens surface. The separation distance, d_2, between the UC-PBG layers is approximately half the focal length (or $\lambda/4$ at the operating resonant frequency) as shown in Figure 3. Furthermore, the emerged electromagnetic beam from the UC-PBG lens is a Gaussian beam which is independent of the azimuth angle [10].

3.2. Design Parameters

The dimensions of the octagon aperture (a and b), periodicity of the UC-PBG layer in both the x- and y-directions (X and Y), the periodical repetitions (m and n) in the x- and y-directions, separation

distances between the UC-PBG layers and the radiating elements (d_1 and d_2) and number of the UC-PBG layers (S_o) are listed in Table 1. The UC-PBG structure has been selected to achieve the maximum gain at 2.6 GHz [10]. The radiating element is a square microstrip antenna printed on a Taconic substrate (relative permittivity = 2.65) and fed with a 50 Ω port with the dimensions listed in Table 2. It should

Table 1. UC-PBG structures dimensions.

Parameter Name	Dimensions
a	14.91 mm
b	36 mm
X	40 mm
Y	40 mm
d_1	30.3 mm
d_2	40 mm
m	9
n	9
S_o	2

Table 2. Microstrip antenna dimensions.

Part Name	Dimensions
Rectangular patch	$41 \times 33.6\,\text{mm}^2$
Substrate	$360 \times 360\,\text{mm}^2$
Ground	$360 \times 360\,\text{mm}^2$
X_f	177 mm
Y_f	180 mm

Table 3. UC-PBG dimensions.

Parameter Name	Dimensions
ρ	40 mm
X	40 mm
Y	40 mm
d_1	30.3 mm
d_2	40 mm
m	9
n	9
S_o	2

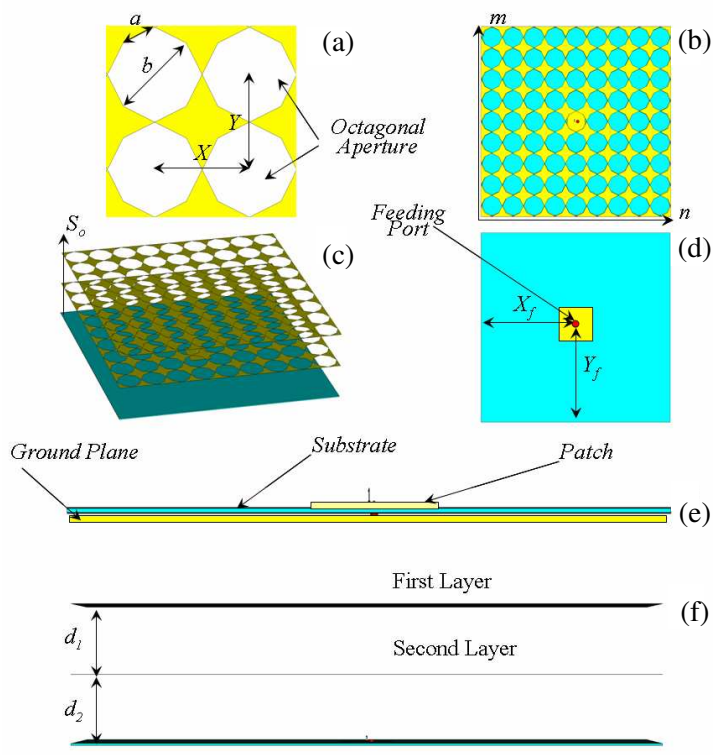

Figure 4. Geometry of the UC-PBG/ antenna. (a) Octagonal apertures; (b) top view of the UC-PBG structure and antenna; (c) 3D geometry of the UC-PBG structure and antenna; (d) top view of the antenna with feed position; (e) side view of the antenna; (f) side view of the antenna with UC-PBG layers.

be noted that in [10] we did not elaborate on the method used for selecting the dimensions of the octagon aperture since the focus was on determining the distance between the two UC-PBG layers based on ray tracing. In this paper, the UC-PBG lens consisting of circular apertures as presented in [11] and shown in Figure 5 is also considered to validate the FDA algorithm. Geometrical details of Figure 5 are summarized in Table 3.

4. RESULTS AND DISCUSSION

In this section, simulation based on time domain solver of CST MWS [13] is presented to validate the FDA algorithm described in Section 2 for the UC-PBG structures introduced in Section 3.

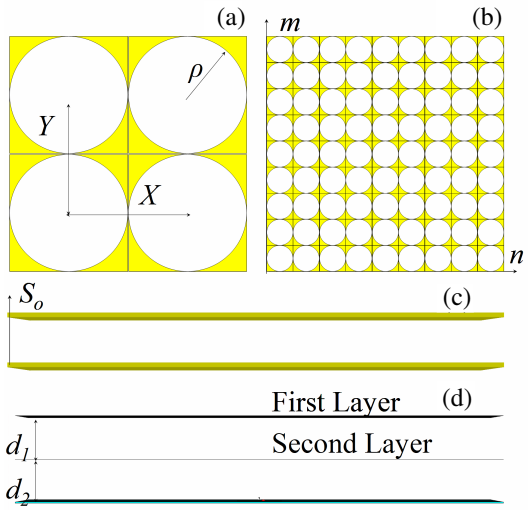

Figure 5. Geometry of the UC-PBG/ antenna. (a) Circular apertures; (b) top view of the UC-PBG structure and antenna; (c) side view of the UC-PBG layers; (d) side view of the antenna with UC-PBG layers.

4.1. Numerical Simulations of the Microstrip Antenna with and without UC-PBG

We have conducted numerous numerical experiments to simulate the UC-PBG structures shown in Figures 4 and 5 without conducting dielectric and metallic losses. Steady state in CST MWS is based on a -80 dB energy decay criterion, while the convergence criterion for the relative deviation of S_{11}, $\Delta S_{11}(f)$ between two consecutive mesh passes was set below 2%. The numerical simulation in terms of S_{11} and directivity versus the elevation angle θ for an azimuth angle φ of 0° are shown in Figure 6 for the octagonal and circular apertures.

4.2. Results from the FDA Algorithm and Ray Tracing Analysis

The directivities of the UC-PBG structures are calculated using the FDA algorithm and compared against full wave 3-D numerical simulations as depicted in Figures 7(a) and (b). An excellent agreement is observed for both cases. The required time to get the directivity using the FDA algorithm is less than 1 sec, while the execution time consumed by CST MWS is about 5 hours using a computer of a 3 GHz CPU and 16 GB of RAM. As shown in Figures 7(c) and (d), the

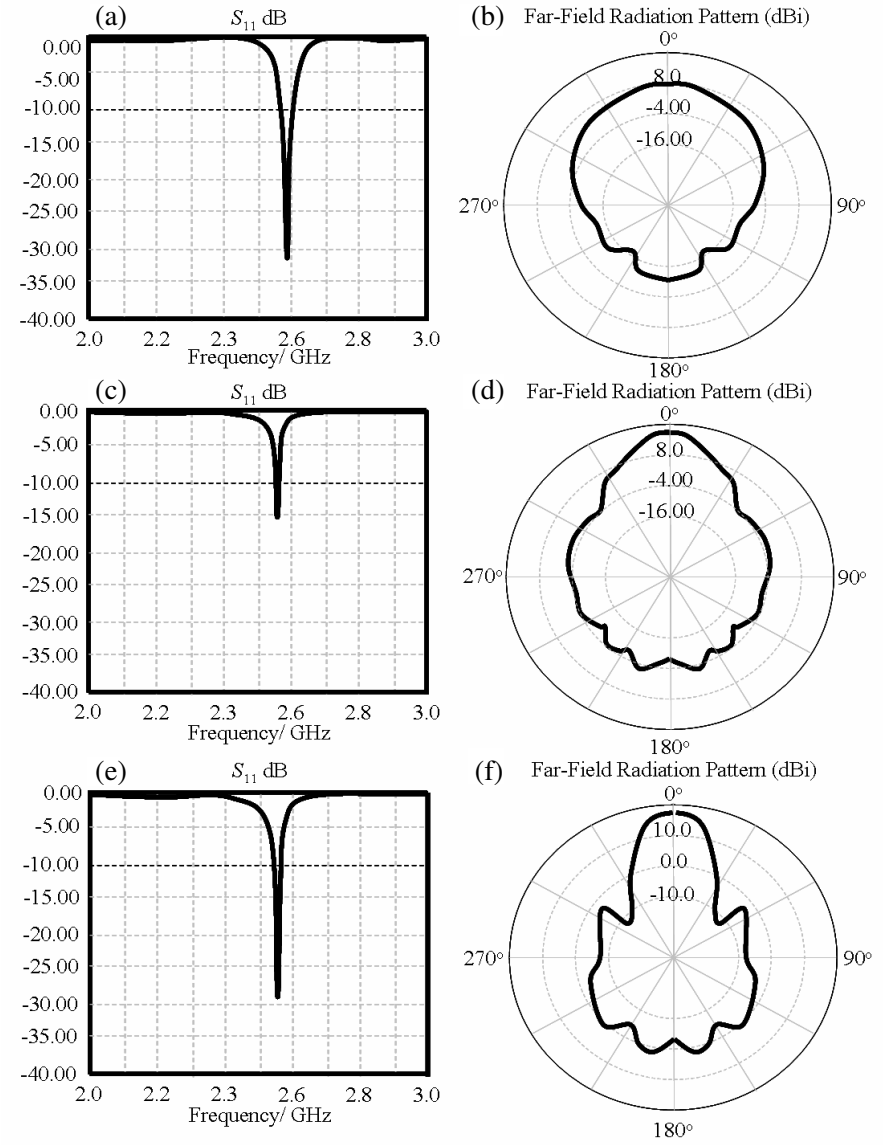

Figure 6. S_{11} spectra and directivity of the combination of the UC-PBG layers and microstrip antenna versus elevation angle ($\theta = -180°$ to 180°), azimuth angle ($\varphi = 0°$). (a) S_{11} and (b) directivity for conventional antenna; (c) S_{11} and (d) directivity for the octagonal aperture; and (e) S_{11} and (f) directivity for the circular aperture.

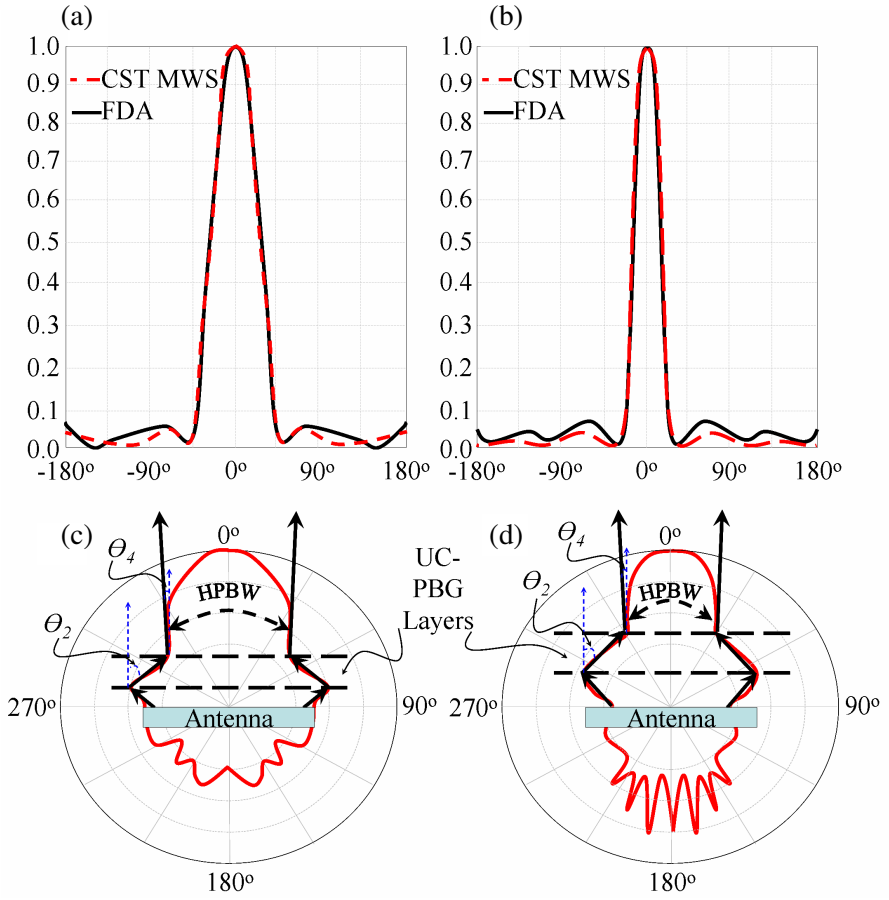

Figure 7. Normalized directivity of the combination of the UC-PBG layers and microstrip antenna based on the FDA algorithm and CST MWS versus elevation angle ($\theta = -180°$ to $180°$), azimuth angle ($\varphi = 0°$). (a) and (b) for the octagonal and circular apertures; (c) and (d) for the octagonal and circular apertures based ray tracing compared to the numerical results of the radiation pattern.

refraction angle of the incident radiation is changed from 35° to 2° for the octagonal aperture and to 0.5° for the circular aperture. This implies that the rays are almost normal to the lens, which leads to maximum achievable gain as explained by Equation (20). At this angle, the refractive index of the second layer n_2 is less than -1 and for the

Table 4. The HPBW of the emerged electromagnetic beam before and after introducing the UC-PBG structures.

Solver	*UC-PBG* (*Octagonal*)	*UC-PBG* (*Circular*)
CST MWS	23°	17°
FDA algorithm	25°	18°

first layer, $0 < n_1 < 1$ as described by Snell's law in Equation (21).

$$D_o \approx \frac{4\pi}{\Theta\Phi} \tag{20}$$

$$n_1 \sin(\theta_1) = n_2 \sin(\theta_2) \tag{21}$$

where, D_o is the maximum directivity, Φ and Θ are the HPBW solid angles at the elevation and azimuth directions, θ_1 and θ_2 are the angle of incidence and refraction, respectively. In Table 4, the HPBW angles are given for both UC-PBG structures from the ray tracing analysis.

5. CONCLUSIONS

In this paper, a novel algorithm is presented which combines FO and DSP concepts to predict the far field radiation pattern of two different UC-PBG structures based on circular and octagonal apertures. Rigorous 3-D fullwave simulations are conducted using CST MWS to evaluate the performance of the UC-PBG/ antenna structures and to validate the FDA algorithm. An excellent agreement has been observed among results obtained from rigorous 3D electromagnetic simulations and those evaluated from the FDA algorithm. We have found that it is possible to treat the UC-PBG structures as an array of spatial filters of certain IR calculated using FO. Furthermore, the periodicity of the UC-PBG structures can be treated using the sampling theorem which is inspired from a DSP approach. Finally, the proposed algorithm can be used as an optimization tool to infer the UC-PBG dimensions necessary to realize the maximum gain at the appropriate resonant frequency of a microstrip antenna.

APPENDIX A.

Proof of Equation (2):

Consider the impulse response of the UC-PBG layer given by

$$f_{SL}[x, y] = \sum_{n=-N/2}^{N/2} \sum_{m=-M/2}^{M/2} f_{uc}(x - nX,\, y - mY) \tag{A1}$$

Equation (A1) can be written as

$$f_{SL}\left[x,y\right] = f_{uc}\left(x,y\right) \sum_{n=-N/2}^{N/2} \sum_{m=-M/2}^{M/2} \delta(x - nX,\, y - mY) \qquad \text{(A2)}$$

where δ is the Dirac delta function.

Taking the Fourier transform of Equation (A2), we obtain

$$\begin{aligned} F_{SL}[v_x, v_y] &= F_{uc}\left(v_x, v_y\right) \sum_{-N/2}^{N/2} \sum_{-M/2}^{M/2} e^{-j(nX2\pi v_x + mY2\pi v_y)} \\ &= F_{uc}(v_x, v_y) \left[\sum_{-N/2}^{N/2} e^{-jnX2\pi v_x}\right] \left[\sum_{-M/2}^{M/2} e^{-jmY2\pi v_y}\right] \end{aligned} \qquad \text{(A3)}$$

where F_{SL} is the Fourier transform of f_{SL}.

Each geometric series in the brackets of Equation (A3) can be evaluated as

$$\sum_{-N/2}^{N/2} e^{-j\frac{n}{X}2\pi v_x} = \frac{\sin(\pi v_x(N+1)X)}{\sin(\pi v_x X)} \qquad \text{(A4)}$$

Replacing Equation (A4) in Equation (A3), we obtain the desired expression for the frequency response

$$F_{SL}(v_x, v_y) = F_{uc}(v_x, v_y) \left[\frac{\sin(\pi v_x(N+1)X)}{\sin(\pi v_x X)}\right] \left[\frac{\sin(\pi v_y(M+1)Y)}{\sin(\pi v_y Y)}\right] \qquad \text{(A5)}$$

REFERENCES

1. Joannopoulos, J. D., S. G. Johnson, J. N. Winn, and R. D. Meade, *Photonic Crystals: Molding the Flow of Light*, 2nd Edition, Princeton University Press, 2008.
2. Zhan, L. and Y. Rahmat Samii, "PBG, PMC, and PEC ground planes: A case study dipole antennas," *International Symposium on Antennas and Propagation*, 674–677, Salt Lake City, UT, 2000.
3. Zhao, Y. and C. G. Parini, "A 30 GHz dual linear polarized microstrip antenna array and its characteristics on PBG substrate," *31st European Microwave Conf.*, Vol. 2, 29–32, London, 2001.
4. Caloz, C., C. C. Chang, and T. Itoh, "A novel anisotropic uniplanar compact photonic band-gap (UC-PBG) ground plane," *31st European Microwave Conf.*, Vol. 2, 185–187, London, 2001.

5. Kuo, Y. L., T. W. Chiou, and K. L. Wong, "A dual-band rectangular microstrip antenna using a novel photonic band gap ground plane of unequal orthogonal periods," *Microw. Opt. Techn. Lett.*, Vol. 30, 280–283, 2001.
6. Sauleau, R., P. Coquet, T. Matsui, and J.-P. Daniel, "A new concept of focusing antennas using plane-parallel Fabry-Perot cavities with nonuniform mirrors," *IEEE Trans. Ant. Prop.*, Vol. 51, 3171–3175, 2003.
7. Hao, Y., A. H. Alomainy, and C. G. Parini, "Antenna-beam shaping from offset defects in UC-EBG cavities," *Microw. Opt. Techn. Lett.*, Vol. 43, 108–112, 2004.
8. Weng, Z., N. Wang, and Y. Jiao, "Study on high gain patch antenna with metamaterial cover," *ISAPE'06, 7th International Symposium on Antennas, Propagation & EM Theory*, Vol. 34, No. 3, 1–2, Apr. 2007.
9. Elwi, T. A., H. M. Al-Rizzo, D. G. Rucker, and F. Song, "Numerical simulation of a UC-PBG lens for gain enhancement of microstrip antennas," *International Journal of RF and Microwave Computer-Aided Engineering*, Vol. 19, No. 6, 676–684, Nov. 2009.
10. Saleh, B. E. A. and M. C. Teich, *Fundamentals of Photonics*, 2nd Edition, John Wiley & Sons, Inc., Hoboken, New Jersey, May 2007.
11. Goodman, J. W., *Introduction to Fourier Optics*, 3rd Edition, McGraw-Hill Companies, Inc., St. Louis San Francisco, New York, Aug. 2005.
12. Balanis, C. A., *Antenna Theory Analysis and Design*, 3rd Edition, John Wiley & Sons, Inc., Hoboken, New Jersey, Apr. 2005.
13. CST Microwave Studio. 10th version. Available: http://www.cst.-com., 2010.